



Surface functionalization of mesoporous silica MCM-41 with 3-aminopropyltrimethoxysilane for dye removal: kinetic, equilibrium, and thermodynamic studies

Jin-Kyu Kang^a, Jeong-Ann Park^a, Jae-Hyun Kim^a, Chang-Gu Lee^b, Song-Bae Kim^{a,c,*}

^a*Environmental Functional Materials & Biocolloids Laboratory, Seoul National University, Seoul 151-921, Republic of Korea, Tel. +82 2 880 4587; Fax: +82 2 873 2087; email: songbkim@snu.ac.kr (S.-B. Kim)*

^b*Center for Water Resource Cycle Research, Korea Institute of Science and Technology, Seoul 136-791, Republic of Korea*

^c*Department of Rural Systems Engineering, Research Institute of Agriculture and Life Sciences, Seoul National University, Seoul 151-921, Republic of Korea*

Received 7 May 2014; Accepted 24 January 2015

ABSTRACT

Mesoporous silica MCM-41 was synthesized and functionalized with a silane coupling agent (3-aminopropyltrimethoxysilane, APTMS) for the removal of Acid Blue 25 (AB25, anionic dye) and Methylene Blue (MB, cationic dye) from aqueous solutions as adsorbents. The synthesized (MCM-41) and functionalized (f-MCM-41) materials were characterized using field emission scanning electron microscopy, energy-dispersive X-ray spectrometry, transmission electron microscopy, particle size analysis, nitrogen gas adsorption-desorption analysis, X-ray diffraction spectrometry, and Fourier transform infrared spectrometry. The results indicate that the surface modification of MCM-41 with APTMS was successfully carried out. Batch experiments were performed to examine AB25 and MB removal by MCM-41 and f-MCM-41 under various experimental conditions. The results show that f-MCM-41 was a good adsorbent for anionic AB25, but not for cationic MB. This could be attributed to the presence of amine groups on the surfaces of f-MCM-41 from the APTMS modification. Conversely, MCM-41 was good for MB removal, but not for AB25 removal. AB25 removal in f-MCM-41 was sensitive to solution pH, with decreasing adsorption capacity as pH increased from 4.1 to 9.4. MB removal in MCM-41 was sensitive to solution pH in the opposite manner, with increasing adsorption capacity as pH increased from 4.1 to 10.3. Thermodynamic analysis showed that the adsorption of AB25 to f-MCM-41 and of MB to MCM-41 decreased with increasing temperature from 15 to 45°C, indicating the exothermic nature of the sorption process. This study demonstrated that surface functionalization with silane coupling agents can help to make MCM-41 useful for the removal of various types of dyes.

Keywords: Dye removal; MCM-41; Mesoporous silica; Silane coupling agent; Surface functionalization

*Corresponding author.

1. Introduction

Pollution of water bodies by effluents from the textile industry is a serious environmental problem. Dyes released from textile effluents impart a significant color to water, making consumption unfeasible. In addition, dyes reduce the transmission of sunlight through water, affecting the photosynthesis of aquatic plants. Furthermore, dyes pose a great threat to aquatic life and human beings due to their mutagenic and carcinogenic properties [1]. Therefore, the removal of dyes from textile effluents is a contentious topic in environmental research.

Various treatment techniques have been used for the removal of dyes from water, including adsorption, sedimentation, flotation, flocculation, coagulation, foam fractionation, ionizing radiation, incineration, filtration, neutralization, reduction, oxidation, electrolysis, ion exchange, advanced oxidation processes, stabilization ponds, aerated lagoons, trickling filters, and activated sludge [1]. Among these processes, adsorption is the most widely applied, mainly because of cost-effectiveness and simplicity of operation. Several adsorbents have been tested for dye removal, including activated carbon, alumina, silica gel, and zeolite [2–4].

Mesoporous silica is a form of silica with large pore diameters, ranging from 2 to 50 nm. Mesoporous silica has a large surface area with high chemical and thermal stability. The most common types of mesoporous silica materials are Mobil Crystalline of Materials 41 (MCM-41) and Santa Barbara Amorphous 15 (SBA-15). Mesoporous silica and surface-modified mesoporous silica have been used as adsorbents for dye removal from aqueous solutions [5–7]. A silane coupling agent is a bifunctional compound composed of two functionally active end groups (hydrolyzable and organofunctional). The hydrolyzable group reacts chemically with the silanol groups on the surfaces of silica to form stable siloxane bonds, whereas the organofunctional group provides desired surface characteristics or reactive groups [8,9]. Recently, silane coupling agents have been used by several researchers [10–13] to accommodate functional groups (amine, carboxylic, decyl, phenyl, and sulfonic acid) on the surfaces of mesoporous silica through surface modification for the removal of various types of dyes. For example, Anbia and Salehi [14] used ethylenediamine-, aminopropyl-, and pentaethylenhexamine-functionalized SBA-3 mesoporous silica for the adsorption of acid dyes. Fu et al. [15] functionalized superparamagnetic mesoporous silica microspheres with 3-mercaptopropyltriethoxysilane to graft carboxylic groups for the removal of Methylene Blue (MB)

and acridine orange. Cestari et al. [16] modified the surfaces of mesoporous silica gel using 3-(trimethoxysilyl)propylamine to provide amine groups for the removal of yellow and red dyes.

The aim of this study was to characterize the removal of Acid Blue 25 (AB25, anionic dye) and MB (cationic dye) from aqueous solutions using both mesoporous silica MCM-41 and MCM-41 functionalized with a silane coupling agent (3-aminopropyltrimethoxysilane, APTMS) as adsorbents. APTMS contains amine groups, which are considered as functional moieties for dye removal [17], and has shorter linker length than other amine functional silane (e.g. N-(2-aminoethyl)-3-aminopropyltrimethoxysilane) [18], such that surface area reduction effect on mesoporous silica can be much lower when modifying with APTMS [19]. The properties of the synthesized (MCM-41) and functionalized (f-MCM-41) materials were analyzed using various characterization techniques. Batch experiments were performed to examine AB25 and MB removal by MCM-41 and f-MCM-41 under various experimental conditions, including reaction time, dye concentration, solution pH and temperature. Sorption kinetic, equilibrium isotherm, and thermodynamic models were used for the data analysis.

2. Materials and methods

2.1. Synthesis and functionalization of MCM-41

Mesoporous silica MCM-41 was synthesized according to procedures reported in the literature [20]. Briefly, 205 mL of ammonia water (25 weight %, Daejung Chemicals & Metals) was mixed with 270 mL of deionized water (Direct-Q, Millipore) at room temperature. Then, 2.0 g of cetyltrimethylammonium bromide (CTAB, $\geq 99\%$, Sigma-Aldrich) as a template (surfactant) was dissolved into the solution and stirred for 1 h to form hexagonal arrayed micelle rods. Next, 10 mL of tetraethylorthosilicate (TEOS, $\geq 99\%$, Sigma-Aldrich) was added as a silica source. After 2 h of crystallization via stirring, a white precipitate was obtained, filtered, and washed with 2 L of deionized water to neutralize the pH. The washed precipitate was dried under a desiccator overnight, and then calcined at 550 °C in air for 4 h to remove the surfactant. After cooling, MCM-41 powder was obtained via fragmentation with a mortar and pestle.

f-MCM-41 was synthesized using methods modified from the literature [21]. First, 4.0 g of APTMS ($\geq 97\%$, Sigma-Aldrich) as a functional monomer was mixed with 100 mL of methanol and refluxed for 3 h. Then, 6.0 g of MCM-41 powder was added to the mixture, stirred, and refluxed for 24 h. The resulting

precipitate was filtered and washed with 500 mL ethanol to remove the unreacted functional monomer. Next, the precipitate was washed again with 1 L of deionized water, filtered, and dried at 105°C in the air overnight. After cooling, f-MCM-41 powder was obtained via fragmentation with a mortar and pestle.

2.2. Characterization of MCM-41 and f-MCM-41

The characteristics of MCM-41 and f-MCM-41 were determined using field emission scanning electron microscopy (FESEM), energy-dispersive X-ray spectrometry (EDS), transmission electron microscopy (TEM), particle size analysis, nitrogen gas (N₂) adsorption–desorption analysis, X-ray diffraction (XRD) spectrometry, and Fourier transform infrared spectrometry (FTIR). FESEM and EDS analysis and color mapping of MCM-41 and f-MCM-41 were performed using a field emission scanning electron microscope (Supra 55VP, Carl Zeiss, Germany). TEM (JEM-1010, JEOL, Japan) was used to take images of the mesoporous silica. Particle size was analyzed using a Zetasizer (ELSZ-1000, Otsuka Electronics, Japan). N₂ adsorption–desorption analysis was performed using a surface area analyzer (BELSORP-max, BEL Japan Inc., Japan) after the sample was pretreated at 120°C. From the N₂ adsorption–desorption isotherms, the specific surface area, average pore diameter, total pore volume, and mesopore volume were determined by Brunauer–Emmett–Teller (BET) and Barrett–Joyner–Halenda (BJH) analyses. The mineralogical and crystalline structural properties were examined using low-angle XRD (D8 Discover, Bruker, Germany) with a CuK α radiation of 1.5406 Å at an exposure time of 1,800 s. Infrared spectra were recorded on a Bomem MB-104 (Abb-Bomem Inc., Quebec, Canada) FTIR spectrometer using KBr pellets.

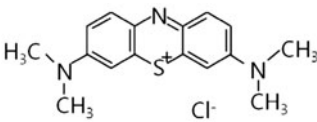
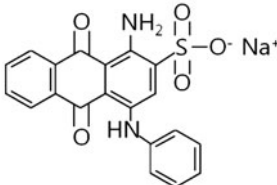
2.3. Dye removal experiments

Batch experiments were performed in solution containing AB25 (Sigma-Aldrich, 210,684) or MB (Sigma-Aldrich, M44907). The characteristics of AB25 and MB are summarized in Table 1. The desired dye solution was prepared by diluting the stock solution (1,000 mg L⁻¹). Batch experiments were performed at 30°C unless stated otherwise. All of the experiments were performed in triplicate.

The first experiments were conducted to observe the effect of reaction time on dye removal, and 0.05 g of adsorbent (MCM-41 or f-MCM-41) was added to 50 mL of dye solution (initial concentration = 100 mg L⁻¹). The solutions were shaken in a shaking incubator at 150 rpm and 25°C. The samples were collected at regular time intervals and filtered through a 0.45 μ m membrane filter. The dye concentration was measured by a UV–visible spectrometer (Aquamate, Thermo). The characteristic wavelengths of 600 nm for AB25 and 665 nm for MB were selected for the analysis. Both signals displayed good linear relationships between intensity and concentration. Additional experiments (adsorbent dose = 0.05 g L⁻¹; initial concentration = 100 mg L⁻¹) were performed at 15 and 45°C for thermodynamic analysis.

The second experiments were performed to examine the effect of initial dye concentration, and 0.05 g of adsorbent was added to 50 mL dye solution (initial concentration = 10–500 mg L⁻¹). The samples were collected 2 h after the reaction. The third experiments were performed to examine dye removal as a function of solution pH (adsorbent dose = 0.05 g L⁻¹; initial concentration = 100 mg L⁻¹). In these experiments, solution pH was adjusted with 0.1 M HCl and 0.1 M NaOH. The pH was measured with a pH probe (9107BN, Orion, USA).

Table 1
Characteristics of the dyes used in the experiments

General name	Abbreviation	Molecular formula	Structure	λ_{\max} (nm)
Methylene Blue	MB	C ₁₆ H ₁₈ C ₁ N ₃ S		291,665
Acid Blue 25	AB25	C ₂₀ H ₁₃ N ₂ NaO ₅ S		257,600

2.4. Data analysis

All of the parameters of the models were estimated using MS Excel 2010 with the solver add-in function incorporated into the program. The model parameter values were determined by nonlinear regression. The determination coefficient (R^2), chi-square coefficient (χ^2), and sum of square error (SSE) were used to analyze the data and confirm the fit to the model. The expressions of R^2 , χ^2 , and SSE are given below:

$$R^2 = \frac{\sum_{i=1}^m (y_c - \bar{y}_c)_i^2}{\sum_{i=1}^m (y_c - \bar{y}_c)_i^2 + \sum_{i=1}^m (y_c - y_e)_i^2} \quad (1)$$

$$\chi^2 = \sum_{i=1}^m \left[\frac{(y_e - y_c)^2}{y_c} \right]_i \quad (2)$$

$$SSE = \sum_{i=1}^m (y_e - y_c)_i^2 \quad (3)$$

3. Results and discussion

3.1. Characteristics of MCM-41 and f-MCM-41

FESEM images of MCM-41 and f-MCM-41 are presented in Fig. 1, demonstrating that MCM-41 had a sphere or rod-like morphology, and that f-MCM-41 had a similar shape. TEM images (Fig. 2) show that MCM-41 had a hexagonal shape with a regular arrangement of pores, and that the surface of f-MCM-41 was covered with APTMS. The physical characteristics of MCM-41 and f-MCM-41 are presented in Table 2. The particle size analysis indicates that f-MCM-41 had a size of 585.7 ± 105.6 nm, which was larger than MCM-41 (527.9 ± 100.1 nm).

N_2 adsorption–desorption isotherms for MCM-41 and f-MCM-41 are illustrated in Fig. 3(a). The BET surface area of MCM-41 was determined to be $1239.5 \text{ m}^2 \text{ g}^{-1}$ with a total pore volume of $0.917 \text{ cm}^3 \text{ g}^{-1}$, average pore diameter of 2.97 nm, and mesopore volume of $0.848 \text{ cm}^3 \text{ g}^{-1}$. For f-MCM-41, the BET surface area was $509.9 \text{ m}^2 \text{ g}^{-1}$ with a total pore volume of $0.342 \text{ cm}^3 \text{ g}^{-1}$, average pore diameter of 2.69 nm, and

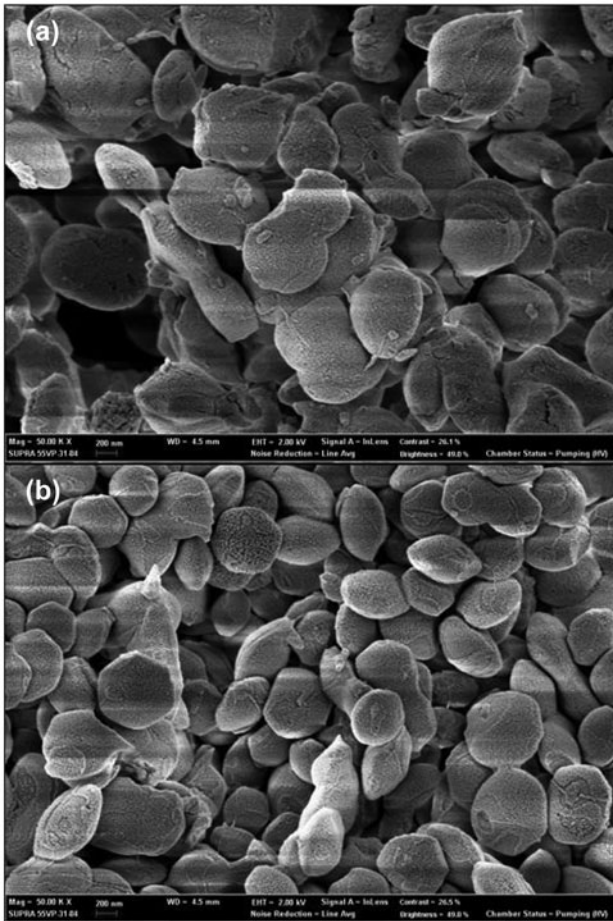


Fig. 1. FESEM images of mesoporous silica: (a) MCM-41 (bar = 200 nm) and (b) f-MCM-41 (bar = 200 nm).

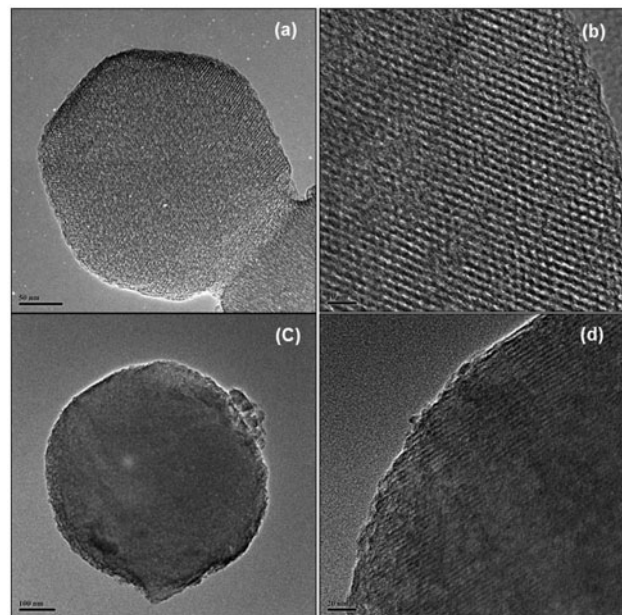


Fig. 2. TEM images of mesoporous silica: (a) MCM-41 (bar = 50 nm); (b) MCM-41 (bar = 10 nm); (c) f-MCM-41 (bar = 50 nm); and (d) f-MCM-41 (bar = 10 nm).

Table 2

Physical characteristics of the mesoporous silica synthesized in the laboratory (data from particle size analysis and N₂ adsorption–desorption analysis)

Mesoporous silica	Particle size (nm)	BET surface area (m ² g ⁻¹)	Total pore volume (cm ³ g ⁻¹)	Average pore diameter (nm)	Mesopore volume (cm ³ g ⁻¹)
MCM-41	527.9 ± 100.1	1239.5	0.917	2.96	0.848
f-MCM-41	585.7 ± 105.6	509.9	0.342	2.69	0.221

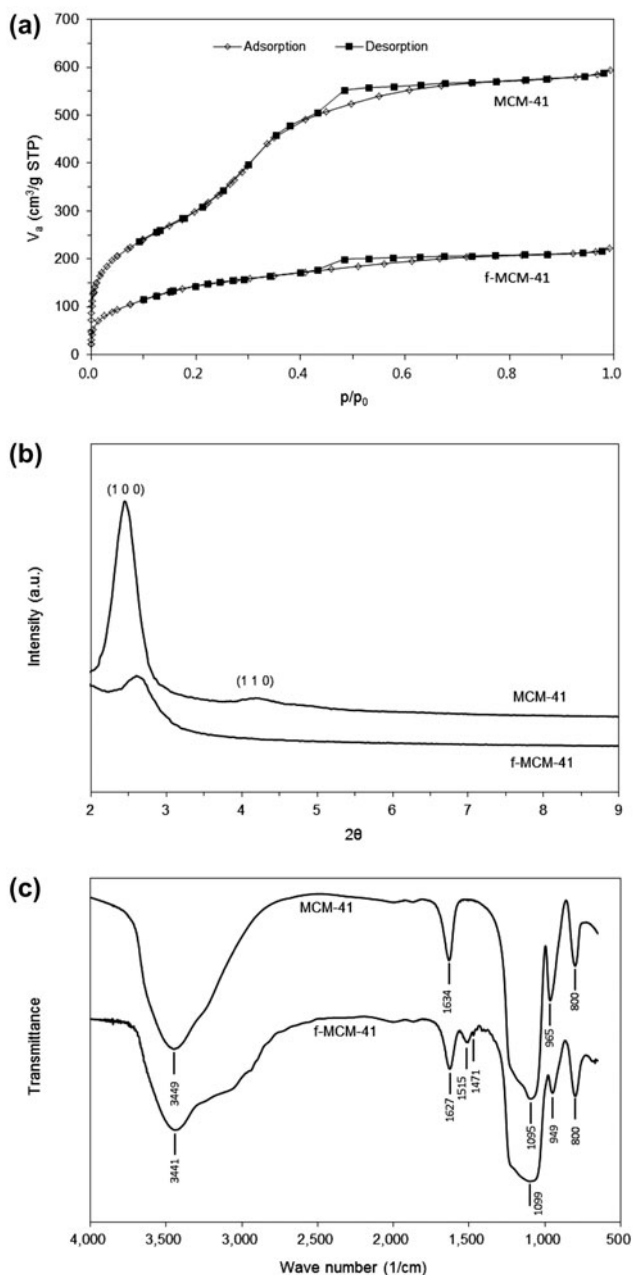


Fig. 3. N₂ adsorption–desorption isotherms (a) low-angle XRD patterns and (b) FTIR spectra of mesoporous silica (MCM-41 and f-MCM-41).

mesopore volume of 0.221 cm³ g⁻¹ (Table 2). Compared with MCM-41, the BET surface area and other values of f-MCM-41 were reduced due to the surface modification. Low-angle XRD patterns of MCM-41 and f-MCM-41 are shown in Fig. 3(b). The XRD pattern of MCM-41 indicates two peaks at $2\theta = 2.44$ and 4.18 , and these peaks were indexed to (100) and (110) reflections, respectively, a characteristic of hexagonal mesostructures [22]. The XRD pattern of f-MCM-41 demonstrates that the main peak signal of MCM-41 existed in f-MCM-41. The shift of (100) diffraction peak to the right in f-MCM-41 could be attributed to the decrease of pore size as a result of amine groups anchoring on the mesopores of MCM-41 [22]. In the FTIR spectra of MCM-41 (Fig. 3(c)), a broad band around 3449 cm^{-1} along with the peaks at $1,634$ and 965 cm^{-1} corresponded to the vibration bands of silanol groups (Si–OH), which are involved in the surface modification with silane coupling agents [8]. The bands at $1,095$ and 800 cm^{-1} were attributed to the stretching vibration of Si–O–Si groups. The FTIR data of f-MCM-41 show the major bands found in the FTIR spectra of MCM-41. Particularly in the FTIR data of f-MCM-41, the vibration bands of amine groups ($-\text{NH}_2^+$) were found at $1,515$ and $1,471\text{ cm}^{-1}$ (Fig. 3(c)).

EDS patterns of MCM-41 and f-MCM-41 are presented in Fig. 4. Silicon (Si) was the major element of MCM-41 with a weight percent of 38.58% (Fig. 4(a)). In the EDS pattern of f-MCM-41 (Fig. 4(b)), nitrogen (N) appeared due to the surface modification by ATPMS. Through EDS analysis, Si was evident at the peak position of 1.740 keV as the K alpha X-ray signal. In f-MCM-41, N was evident at the peak position of 0.392 keV as the K alpha X-ray signal. Color mapping was performed to visualize the spatial distribution of Si and N on f-MCM-41 (Fig. 5). Si was colored yellow-green (Fig. 5(b), (d)), whereas N was visualized as green (Fig. 5(c), (d)). The results indicate that the surface modification of MCM-41 with the silane coupling agent (APTMS) was successfully carried out.

3.2. Characteristics of AB25 and MB removal

The effect of reaction time on the removal of AB25 and MB by MCM-41 and f-MCM-41 is shown in

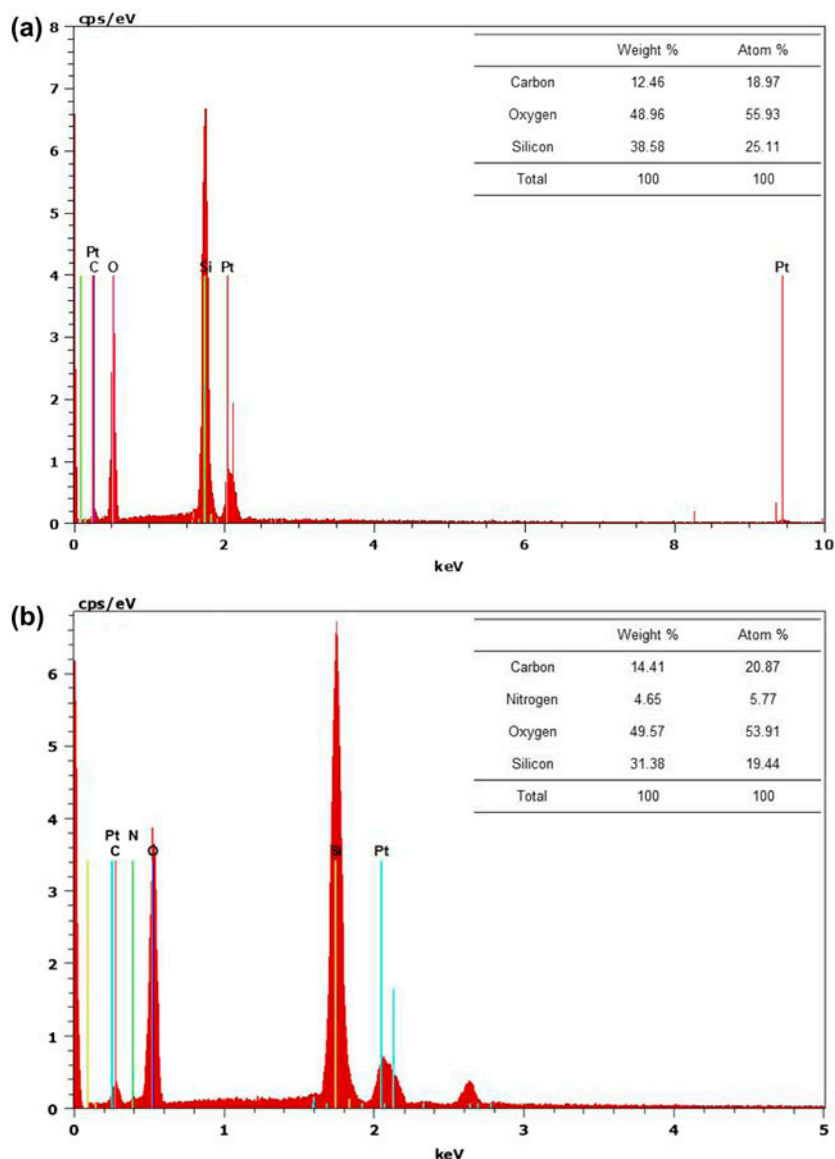


Fig. 4. EDS patterns of mesoporous silica: (a) MCM-41 and (b) f-MCM-41.

Fig. 6. In the case of MCM-41, the adsorption capacity of MB was 43.4 mg g^{-1} at 5 min of reaction time, increased to 48.5 mg g^{-1} at 15 min, and then remained relatively constant thereafter. The adsorption of MB to MCM-41 reached the equilibrium very fast, mainly due to high BET surface area along with uniformity of two-dimensional hexagonal cylindrical pores of MCM-41 [23]. The adsorption capacity of AB25 was far lower than that of MB. The adsorption capacity of AB25 was 1.8 mg g^{-1} at 30 min, which was only 4% of MB (48.9 mg g^{-1}) at the same reaction time. In the case of f-MCM-41, the adsorption capacity of AB25 was 18.3 mg g^{-1} at 5 min and increased to 19.9 mg g^{-1} at 10 min. The adsorption capacity of MB was far lower

than that of AB25 and was determined to be 3.6 mg g^{-1} at 30 min only 18% of AB25 (20.1 mg g^{-1}) at the same reaction time.

Our results indicate that the adsorption of MB to MCM-41 was favorable, whereas the adsorption of AB25 to MCM-41 was not. Conversely, the adsorption of AB25 to f-MCM-41 was favorable, whereas the adsorption of MB to f-MCM-41 was not. These phenomena could be attributed to the fact that MB is a cationic dye, and so, the adsorption of positively charged MB to negatively charged MCM-41 was favorable under the experimental conditions (pH 6.0) due to electrostatic attraction [22,24]. The pH_{pzc} of MCM-41 was determined to be 4.0, above which the

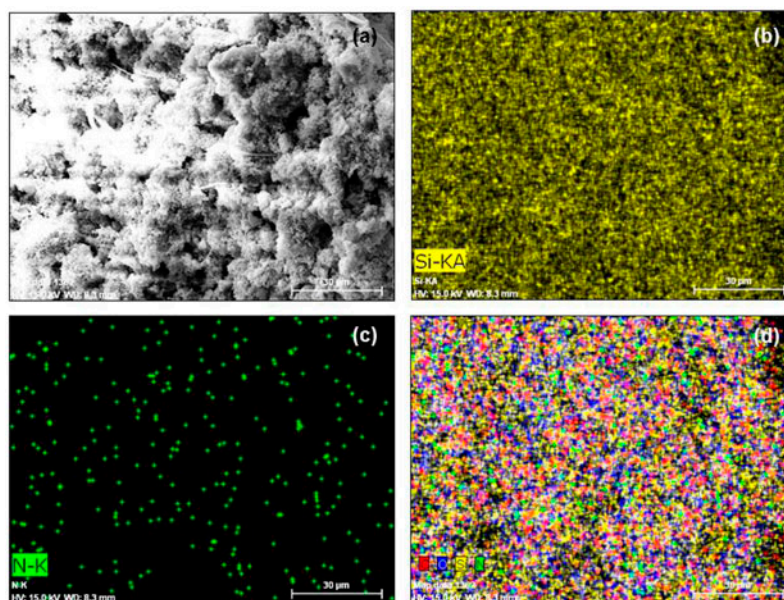


Fig. 5. Color mapping of mesoporous silica f-MCM-41: (a) FESEM image (bar = 30 μm); (b) Si map; (c) N map; and (d) overlay of the secondary electron image, Si map and N map.

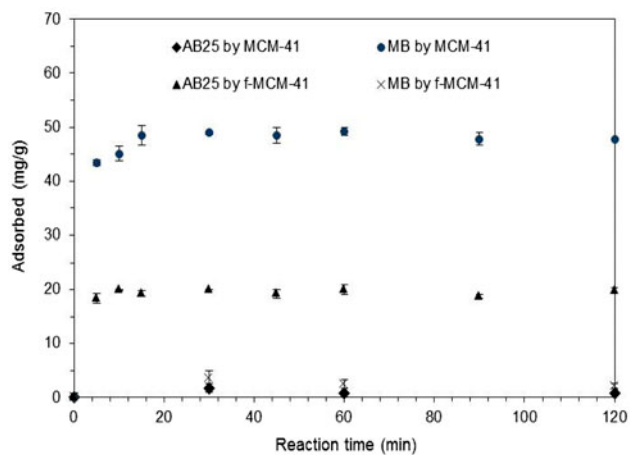


Fig. 6. Effect of reaction time on the removal of AB25 and MB by mesoporous silica MCM-41 and f-MCM-41 (initial dye concentration = 100 mg L^{-1}).

surface of MCM-41 is negatively charged. Conversely, the adsorption of negatively charged AB25 to MCM-41 was not favorable under the experimental conditions (pH 5.6) due to electrostatic repulsion. The hydroxyl groups ($-\text{OH}^-$) on the surfaces of MCM-41 could not provide strong sorption sites for negatively charged AB25.

When the surfaces of f-MCM-41 were covered by amine groups via APTMS modification, the adsorption of AB25 to f-MCM-41 became favorable because

the number of positively charged sorption sites increased. The adsorption of negatively charged AB25 to f-MCM-41 was enhanced due to electrostatic attraction. Conversely, the adsorption of positively charged MB to f-MCM-41 became unfavorable due to electrostatic repulsion.

Our results conform well to the reports of other researchers who demonstrated that negatively charged mesoporous silica was effective in the removal of cationic MB. Anbia and Hariri [24] reported that mesoporous silica SBA-3 was effective for the adsorption of MB through electrostatic attraction. Dong et al. [25] demonstrated that mesoporous silica SBA-15 was an excellent adsorbent for MB in aqueous solutions. Wang and Li [6] also showed the effective adsorption of MB to MCM-41, MCM-48, and MCM-50, and the latter demonstrated higher adsorption. Researchers have also reported that the adsorption capacity of mesoporous silica for anionic dyes could be improved via surface functionalization. Ho et al. [10] reported that amino-containing MCM-41 had a strong affinity for AB25, whereas carboxylic-containing MCM-41 displayed a large sorption capacity for MB. Anbia and Salehi [14] showed that amino-functionalized SBA-3 effectively removed acid dyes (AB113, Acid Red 114, Acid Green 28, Acid Yellow 127, and Acid Orange 67), due to the electrostatic attraction between the positively charged amine groups on the silica surfaces and the negatively charged sulfonate groups ($-\text{SO}_3^-$) of the acid dyes.

The effect of AB25 and MB concentration on dye removal is presented in Fig. 7. MB removal by MCM-41 was highly concentration-dependent. At the lowest concentration of 10 mg L^{-1} , the adsorption capacity was 9.0 mg g^{-1} , which increased to 102.9 mg g^{-1} at the highest concentration of 500 mg L^{-1} . At lower concentrations, the dyes available in the solution are fewer in number than the sorption sites on the adsorbent, and the available dye increased with increasing dye concentrations. However, the adsorption capacity of AB25 in MCM-41 was very low, increasing from 0.05 to 10.8 mg g^{-1} with increasing dye concentrations from 10 to 500 mg L^{-1} , respectively. At dye concentrations of 500 mg L^{-1} , the adsorption capacity of AB25 in MCM-41 was only 10% of the adsorption capacity of MB. In f-MCM-41, the AB25 removal was also highly dependent on concentration. The adsorption capacity was 2.1 mg g^{-1} at the lowest concentration of 10 mg L^{-1} , and increased to 36.8 mg g^{-1} at the highest concentration of 500 mg L^{-1} . The adsorption capacity of MB was very low, increasing from 1.23 to 9.1 mg g^{-1} with increasing dye concentrations from 10 to 500 mg L^{-1} , respectively. At dye concentrations of 500 mg L^{-1} , the adsorption capacity of MB was only 25% of the adsorption capacity of AB25.

The effect of solution pH on the removal of AB25 and MB is demonstrated in Fig. 8. In the case of MCM-41, the adsorption capacity of MB was 33.5 mg g^{-1} at pH 4.1 and increased to 40.5 mg g^{-1} at pH 5.7. As the solution pH increased further and approached 10.3, the adsorption capacity increased to 99.4 mg g^{-1} , indicating that the MB removal by MCM-41 was very sensitive to solution pH changes. In acidic pH, the surfaces of MCM-41 are surrounded

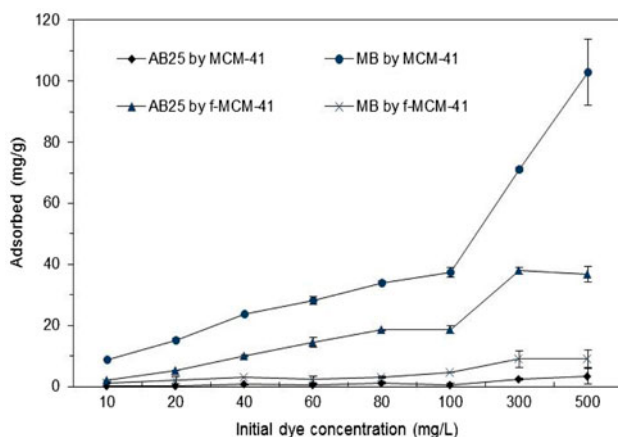


Fig. 7. Effect of dye concentration on the removal of AB25 and MB by mesoporous silica MCM-41 and f-MCM-41 (reaction time = 30 min).

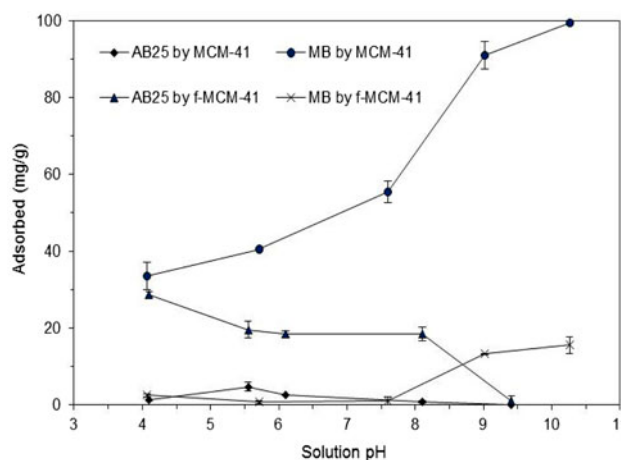


Fig. 8. Effect of solution pH on the removal of AB25 and MB by mesoporous silica MCM-41 and f-MCM-41 (initial dye concentration = 100 mg L^{-1} ; reaction time = 30 min).

by excess H^+ ions, which compete with positively charged MB molecules for the sorption sites on the adsorbent. In alkaline pH, the surfaces of MCM-41 become more negatively charged, due to the presence of excess OH^- ions, resulting in an increase in MB adsorption to MCM-41 via the electrostatic attraction. Our results are similar to the findings of Dong et al. [25] who investigated the effect of solution pH on the removal of MB by SBA-15. They reported that the adsorption of MB to SBA-15 increased slightly with increasing pH from 2 to 6, and then increased sharply in the pH range from 8 to 12. Yan et al. [26] showed that the adsorption capacity of carboxylic-functionalized mesoporous silica for MB increased with increasing pH from 7 to 10. They reported that only part of the carboxylic groups ($-\text{COOH}$) on the surfaces of mesoporous silica are deprotonated at pH 7, whereas all carboxylic groups are present in the form of $-\text{COO}^-$ ions at pH 10, providing more favorable (negatively charged) sorption sites for MB.

In our experiments, the adsorption capacity of AB25 in MCM-41 was below 4.7 mg g^{-1} throughout pH 4.1–9.4. In particular, the adsorption capacity was below 1.0 mg g^{-1} at $\text{pH} > 8.1$. This result could be attributed to the fact that the adsorption of negatively charged AB25 to MCM-41 is not favorable due to electrostatic repulsion. As pH increases to an alkaline condition, the adsorption of AB25 to the surfaces of MCM-41 becomes more unfavorable due to the presence of excess OH^- ions.

In the case of f-MCM-41, the adsorption capacity of AB25 at pH 4.1 was 28.7 mg g^{-1} and decreased to 19.5 mg g^{-1} at pH 5.6. As the pH increased to 8.1, the adsorption capacity decreased slightly to 18.4 mg g^{-1} .

As the pH increased further to 9.4, the adsorption capacity decreased sharply to 1.1 mg g^{-1} , indicating that the removal of AB25 by f-MCM-41 was sensitive to solution pH changes, especially at high pH conditions. In acidic pH, the surfaces of f-MCM-41 are surrounded by excess H^+ ions and became more protonated, resulting in an increase of negatively charged AB25 adsorption to the adsorbent. In alkaline pH, the competition between AB25 and OH^- ions for the sorption sites on f-MCM-41 increases due to the presence of excess OH^- ions, resulting in a decrease of adsorption of AB25 to f-MCM-41. Our results agree well with the report by Asouhidou et al. [11] who investigated the effect of solution pH on the removal of Remazol Red 3BS (anionic) dye by aminopropyl-modified HMS mesoporous silica. The dye removal was more favorable in acidic pH (2.0–4.0), due to the electrostatic attraction between the sulfonate groups of the dye and the protonated amino groups of the mesoporous silica. The removal of Remazol Red 3BS decreased gradually with increasing pH. Anbia and Salehi [14] also showed that the adsorption of acid (anionic) dyes to pentaethylenehexamine-functionalized SBA-3 mesoporous silica decreased with increasing pH from 3.0 to 10.0. In the adsorption process, electrostatic interactions occur between the sulfonate groups of the dyes and the amine groups on the surfaces of SBA-3. Shi et al. [12] also reported that sulfonic acid functionalized hierarchically porous silica adsorbents could effectively remove the positively charged organic compounds (dyes, biogenic amines, pesticides, and amino acids) through electrostatic interactions.

The adsorption capacity of MB to f-MCM-41 was below 2.4 mg g^{-1} at pH 4.1–7.6. This result could be attributed to the fact that the adsorption of positively charged MB to the positively charged surfaces of f-MCM-41 is not favorable at acidic and neutral pH conditions, due to the electrostatic repulsion. The adsorption capacity increased to 13.3 mg g^{-1} at pH 9.0 and to 15.5 mg g^{-1} at pH 10.3. In alkaline pH, the adsorption of MB to f-MCM-41 increases because the number of positively charged sites on the surfaces of f-MCM-41 decrease, whereas the negatively charged sites increase [14]. This result is similar with the report from Fu et al. [15] who investigated the sorption properties of carboxylic functionalized superparamagnetic mesoporous silica microsphere for basic dyes. They reported that carboxylic groups can be easily deprotonated with increasing pH to negatively charged moieties, showing good affinity with basic dyes in high pH. The electrostatic interactions between basic dyes and carboxylic functionalized microsphere could be considered as the major sorption mechanism.

3.3. Kinetics, equilibrium isotherms, and thermodynamic analyses

The reaction time data (MB for MCM-41 and AB25 for f-MCM-41) can be analyzed using the following nonlinear forms of pseudo-first-order, pseudo-second-order, and Elovich kinetic models [27]:

$$q_t = q_e(1 - e^{-k_1 t}) \quad (4)$$

$$q_t = \frac{k_2 q_e^2 t}{1 + k_2 q_e t} \quad (5)$$

$$q_t = \frac{1}{\beta} \ln(\alpha\beta) + \frac{1}{\beta} \ln t \quad (6)$$

where q_t is the amount of dye removed at time t , q_e is the amount of dye removed per unit mass of adsorbent at equilibrium, k_1 is the pseudo-first-order rate constant, k_2 is the pseudo-second-order velocity constant, α is the initial adsorption rate, and β is the adsorption constant.

The kinetic model analyses are presented in Fig. 9, and the kinetic model parameters are provided in Table 3. The values of R^2 , χ^2 , and SSE indicate that the kinetic data were described well by both pseudo-first- and pseudo-second-order models. The values of q_e from the pseudo-first-order model were similar to those from the pseudo-second-order model. For MB sorption to MCM-41, the values of q_e were 48.0–48.6 mg g^{-1} , while they were 19.3 mg g^{-1} for AB25 sorption to f-MCM-41. The rate constant k_2 was used to calculate the initial adsorption rate constant (h) at $t \rightarrow 0$ with the following equation [27]:

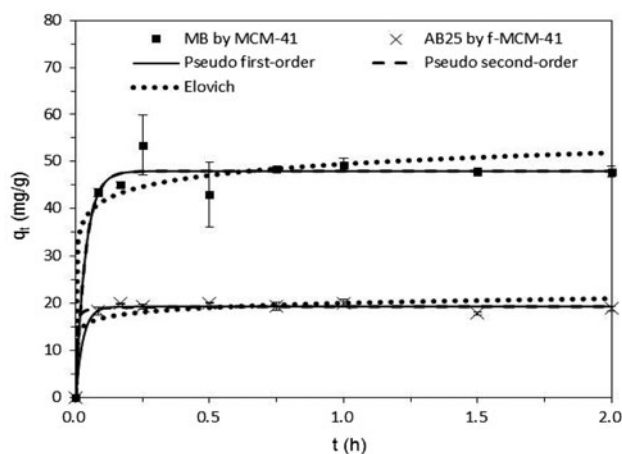


Fig. 9. Kinetic model analysis. Model parameters are provided in Table 3.

Table 3
Kinetic model parameters obtained from model fitting to experimental data

Mesoporous silica	Pseudo-first-order model					Pseudo-second-order model					Elovich model						
	Dye	q_e (mg g ⁻¹)	k_1 (h ⁻¹)	R^2	χ^2	SSE	q_e (mg g ⁻¹)	k_2 (g mg ⁻¹ h ⁻¹)	h (mg g ⁻¹ h ⁻¹)	R^2	χ^2	SSE	α (mg g ⁻¹ h ⁻¹)	β (g mg ⁻¹)	R^2	χ^2	SSE
MCM-41	MB	48.0	27.5	0.969	0.261	63.8	48.5	2.6	6.1E3	0.967	0.241	63.8	5.6E6	0.29	0.936	0.171	129.6
f-MCM-41	AB25	19.3	36.8	0.988	0.243	3.9	19.3	29.2	1.1E4	0.987	0.161	4.5	2.8E6	0.72	0.927	0.160	23.3

$$h = k_2 q_e^2 \tag{7}$$

The values of h were 2–3 orders of magnitude lower than the values of α (initial adsorption rate constant) from the Elovich model.

The dye concentration data (MB for MCM-41 and AB25 for f-MCM-41) can be analyzed using the following nonlinear forms of Langmuir, Freundlich, and Redlich–Peterson isotherm models [28]:

$$q_e = \frac{Q_m K_L C_e}{1 + K_L C_e} \tag{8}$$

$$q_e = K_F C_e^{1/n} \tag{9}$$

$$q_e = \frac{K_R C_e}{1 + a_R C_e^g} \tag{10}$$

where q_e is the amount of dye removed at equilibrium (mg g⁻¹), Q_m is the maximum mass of dye removed per unit mass of adsorbent (removal capacity), K_L is the Langmuir constant related to the binding energy, C_e is the concentration of dye in the aqueous solution at equilibrium, K_F is the distribution coefficient, $1/n$ is the Freundlich constant, K_R is the Redlich–Peterson constant related to the adsorption capacity, a_R is the Redlich–Peterson constant related to the affinity of the binding sites, and g is the Redlich–Peterson constant related to the adsorption intensity.

The equilibrium isotherm model analyses are presented in Fig. 10. The equilibrium model parameters are provided in Table 4. From the Langmuir model,

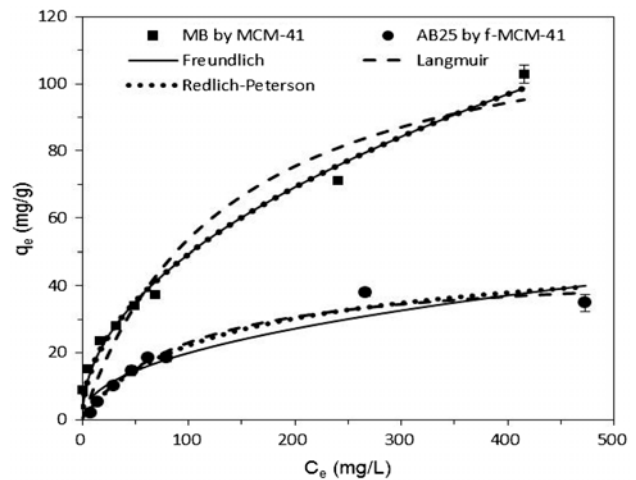


Fig. 10. Equilibrium isotherm model analysis. Model parameters are provided in Table 4.

Table 4
Equilibrium isotherm model parameters obtained from model fitting to experimental data

Mesoporous silica	Freundlich isotherm model					Langmuir isotherm model					Redlich–Peterson model								
	Dye	K_F (L g ⁻¹)	$1/n$	q_m (mg g ⁻¹)	R^2	χ^2	SSE	K (L mg ⁻¹)	Q_m (mg g ⁻¹)	R^2	χ^2	SSE	K_R (L g ⁻¹)	a_R (L mg ⁻¹)	K_R/a_R (mg g ⁻¹)	δ	R^2	χ^2	SSE
MCM-41	MB	5.27	0.49	50.3	0.987	9.386	106.6	0.007	126.1	0.958	178.49	487.6	5.78E+3	1.10E+3	5.27	0.51	0.987	9.405	106.6
f-MCM-41	AB25	2.54	0.45	20.2	0.908	6.732	111.8	0.010	45.9	0.970	1.562	36.1	4.83E-1	1.86E-2	25.9	0.90	0.958	1.887	48.9

the maximum adsorption capacity (Q_m) for MB in MCM-41 was 126.1 mg g⁻¹, which was in the range of the adsorption capacity of mesoporous silica for MB (51.2–285.7 mg g⁻¹) reported in the literature [6,22,25,29]. Additionally, the value of Q_m for AB25 in f-MCM-41 was 45.9 mg g⁻¹, which was similar to or lower than other reported values (55.4 and 145 mg g⁻¹) of functionalized mesoporous silica for AB [30,31]. In the Freundlich isotherm, K_F and $1/n$ can be used to calculate the adsorption capacity q_m with the following equation [32]:

$$q_m = K_F C_0^{1/n} \quad (11)$$

where C_0 is the initial concentration of the dye in the aqueous solution. The values of q_m for MB and AB25 were calculated to be 50.3 and 20.2 mg g⁻¹, respectively. The values of R^2 , χ^2 , and SSE indicate that both the Freundlich and Redlich–Peterson isotherms were suitable for describing the MB equilibrium data, whereas both the Langmuir and Redlich–Peterson isotherms were suitable for the AB25 data.

The thermodynamic analysis was performed using the following equations [33]:

$$\Delta G^\circ = \Delta H^\circ - T\Delta S^\circ \quad (12)$$

$$\Delta G^\circ = \Delta H^\circ - T\Delta S^\circ \quad (13)$$

$$\ln(K_c) = \frac{\Delta S^\circ}{R} - \frac{\Delta H^\circ}{RT}; K_c = \frac{aq_e}{C_e} \quad (14)$$

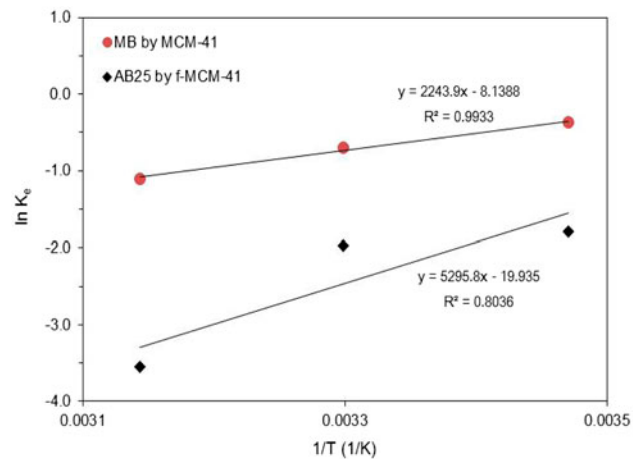


Fig. 11. Thermodynamic analysis. Model parameters are provided in Table 5.

Table 5
Thermodynamic parameters obtained from the experimental data.

Mesoporous silica	Dye	Temp. (°C)	ΔH° (kJ mol ⁻¹)	ΔS° (J K ⁻¹ mol ⁻¹)	ΔG° (kJ mol ⁻¹)
MCM-41	MB	15	-18.66	-67.67	0.84
		30			1.86
		45			2.87
f-MCM-41	AB25	15	-44.03	-167.74	3.73
		30			6.22
		45			8.70

where ΔG° is the change in Gibb's free energy, ΔS° is the change in entropy, ΔH° is the change in enthalpy, R is the gas constant ($=8.314 \text{ J mol}^{-1} \text{ K}^{-1}$), K_e is the equilibrium constant (dimensionless), and a is the adsorbent dose (g L^{-1}). The values of ΔS° and ΔH° were determined by plotting $\ln(K_e)$ vs. $1/T$ using equation (14) and the value of ΔG° was calculated from equation (12).

The thermodynamic analysis for MB adsorption to MCM-41 and AB25 adsorption to f-MCM-41 is presented in Fig. 11. The thermodynamic parameters are provided in Table 5. The negative values of ΔH° represent the exothermic nature of MB adsorption to MCM-41 and AB25 adsorption to f-MCM-41, indicating that adsorption capacity decreases with increasing temperature. The negative values of ΔS° indicate that energy is released during the sorption process and randomness decreases at the interface between solid and solution [22]. In addition, the positive values of ΔG° were obtained for MB adsorption to MCM-41 and AB25 adsorption to f-MCM-41 (Table 5). Similar findings were reported in the literature by Özer et al. [34], who examined the biosorption of Acid Red 337 (AR337) and AB325 (AB325) to seaweed, *Enteromorpha prolifera*, between 303 and 323 K. They obtained the negative parameter values of ΔH° and ΔS° and positive values of ΔG° for biosorption of AR337 and AB325 to the seaweed. They stated that the sorption reaction would always occur until equilibrium is reached regardless of the sign of ΔG° . Karadag et al. [35] also obtained the positive values of ΔG° for the sorption of Reactive Yellow 176 to CTAB and hexadecyltrimethylammonium bromide modified zeolite. According to Karadag et al. [35], the positive values of ΔG° indicate that the amount of dye adsorbed on a solid phase (adsorbent) is lower than the amount of dye in an aqueous phase (solution) at equilibrium. Contrarily, Cestari et al. [16] reported the negative values of ΔG° , indicating the spontaneous sorption process for Reactive Yellow GR and Reactive Red RB on 3-(trimethoxysilyl)propylamine functionalized mesoporous silica.

4. Conclusions

In this study, MCM-41 and f-MCM-41 were used as adsorbents for the removal of AB25 and MB dyes from aqueous solutions. The results show that f-MCM-41 was a good adsorbent for anionic AB25, but not for cationic MB. This could be attributed to the presence of amine groups on the surfaces of f-MCM-41 via the APTMS modification. On the other hand, MCM-41 was good for MB, removal but not for AB25 removal. AB25 removal in f-MCM-41 was sensitive to solution pH with decreasing adsorption capacity from 28.7 to 1.1 mg g^{-1} with increasing pH from 4.1 to 9.4. MB removal in MCM-41 was sensitive to solution pH in the opposite manner, showing increasing adsorption capacity from 33.5 to 99.4 mg g^{-1} with increasing pH from 4.1 to 10.3. Thermodynamic analysis showed that the adsorption of AB25 to f-MCM-41 and of MB to MCM-41 decreased with increasing temperature from 15 to 45°C, indicating the exothermic nature of the sorption process. This study demonstrates that surface functionalization with silane coupling agents can aid in the use of mesoporous silica MCM-41 as an adsorbent for the removal of various types of dyes.

Acknowledgments

This work was supported by the National Research Foundation of Korea, funded by the Ministry of Education, Republic of Korea (grant number 2014-027899).

References

- [1] V.K. Gupta, Suhas, Application of low-cost adsorbents for dye removal—A review, *Environ. Manage.* 90 (2009) 2313–2342.
- [2] T. Robinson, G. McMullan, R. Marchant, P. Nigam, Remediation of dyes in textile effluent: A critical review on current treatment technologies with a proposed alternative, *Bioresour. Technol.* 77 (2001) 247–255.
- [3] G. Crini, Non-conventional low-cost adsorbents for dye removal: A review, *Bioresour. Technol.* 97 (2006) 1061–1085.

- [4] B. Armağan, D.K. Turan, M. Karim, O. Özdemir, M.S. Çelik, Color removal of reactive dyes from water by clinoptilolite, *J. Environ. Sci. Health A*. A39 (2014) 1251–1261.
- [5] P.A. Deshpande, S. Poliset, G. Madras, D. Jyothi, S. Chandrasekaran, Removal of acid dyes from aqueous media by adsorption onto amino-functionalized nanoporous silica SBA-3, *Am. Inst. Chem. Eng.* 58 (2012) 2987–2996.
- [6] S. Wang, H. Li, Structure directed reversible adsorption of organic dye on mesoporous silica in aqueous solution, *Microporous Mesoporous Mater.* 97 (2012) 21–26.
- [7] P.V. Messina, P.C. Schulz, Adsorption of reactive dyes on titania–silica mesoporous materials, *J. Colloid Interface Sci.* 299 (2006) 305–320.
- [8] P. Sae-oui, C. Sirisinha, U. Thepsuwan, K. Hatthapanit, Roles of silane coupling agents on properties of silica-filled polychloroprene, *Eur. Polym. J.* 42 (2006) 479–486.
- [9] M.W. Daniels, J. Sefcik, L.F. Francis, A.V. McCormick, Reactions of a trifunctional silane coupling agent in the presence of colloidal silica sols in polar media, *J. Colloid Interface Sci.* 219 (1999) 351–356.
- [10] K.Y. Ho, G. McKay, K.L. Yeung, Selective adsorbents from ordered mesoporous silica, *Langmuir* 19 (2003) 3019–3024.
- [11] D.D. Asouhidou, K.S. Triantafyllidis, N.K. Lazaridis, K.A. Matis, Adsorption of remazol red 3BS from aqueous solutions using APTES and cyclodextrin-modified HMS-type mesoporous silicas, *Colloid Surf. A*. 346 (2009) 83–90.
- [12] W. Shi, S. Tao, Y. Yu, Y. Wang, M. Ma, High performance adsorbents based on hierarchically porous silica for purifying multicomponent wastewater, *J. Mater. Chem.* 21 (2011) 15567–15574.
- [13] Y. Zhang, Z.A. Qiao, Y. Li, Y. Liu, Q. Hou, Cooperative adsorbent based on mesoporous SiO₂ for organic pollutants in water, *J. Mater. Chem.* 21 (2011) 17283–17289.
- [14] M. Anbia, S. Salehi, Removal of acid dyes from aqueous media by adsorption onto amino-functionalized nanoporous silica SBA-3, *Dyes Pigment.* 94 (2012) 1–9.
- [15] X. Fu, X. Chen, J. Wang, J. Liu, Fabrication of carboxylic functionalized superparamagnetic mesoporous silica microspheres and their application for removal basic dye pollutants from water, *Microporous Mesoporous Mater.* 139 (2011) 8–15.
- [16] A.R. Cestari, E.F.S. Vieira, G.S. Vieira, L.P. Costa, A.M.G. Tavares, W. Loh, C. Airoidi, The removal of reactive dyes from aqueous solutions using chemically modified mesoporous silica in the presence of anionic surfactant—The temperature dependence and a thermodynamic multivariate analysis, *J. Hazard. Mater.* 161 (2009) 307–316.
- [17] S.K. Das, P. Ghosh, I. Ghosh, A.K. Guha, Adsorption of rhodamine B on *Rhizopus oryzae*: Role of functional groups and cell wall components, *Colloid Surf. B*. 365 (2008) 30–34.
- [18] A. Wang, H. Tang, T. Cao, S.O. Salley, K.Y.S. Ng, *In vitro* stability study of organosilane self-assemble monolayers and multilayers, *Colloid Interface Sci.* 343 (2005) 438–447.
- [19] J. Aguado, J.M. Arsuaga, A. Arencibia, M. Lindo, V. Gascón, Aqueous heavy metals removal by adsorption on amine-functionalized mesoporous silica, *J. Hazard. Mater.* 163 (2009) 213–221.
- [20] Q. Cai, W.Y. Lin, F.S. Xiao, W.Q. Pang, X.H. Chen, B.S. Zou, The preparation of highly ordered MCM-41 with extremely low surfactant concentration, *Microporous Mesoporous Mater.* 32 (1999) 1–15.
- [21] R.K. Dey, U. Jha, T. Patnaik, A.C. Singh, V.K. Singh, Removal of toxic/heavy metal ions using ion-imprinted aminofunctionalized silica gel, *Sep. Sci. Technol.* 44 (2009) 1829–1850.
- [22] S. Hamoudi, A. El-Nemr, K. Belkacemi, Adsorptive removal of dihydrogenphosphate ion from aqueous solutions using mono, di- and tri-ammonium-functionalized SBA-15, *J. Colloid Interface Sci.* 343 (2010) 615–621.
- [23] M.A. Zanjanchi, H. Sajjadi, M. Arvand, A. Mohammad-Khah, B. Ghalami-Chooabar, Modification of MCM-41 with anionic surfactant: A convenient design for efficient removal of cationic dyes from wastewater, *CLEAN—Soil Air Water* 39 (2011) 1007–1013.
- [24] M. Anbia, S.A. Hariri, S.N. Ashrafizadeh, Adsorptive removal of anionic dyes by modified nanoporous silica SBA-3, *Appl. Surf. Sci.* 256 (2010) 3228–3233.
- [25] Y. Dong, B.LuS Zang, J. Zhao, X. Wang, Q. Cai, Removal of methylene blue from coloured effluents by adsorption onto SBA-15, *J. Chem. Technol. Biotechnol.* 86 (2011) 616–619.
- [26] Z. Yan, S. Tao, J. Yin, G. Li, Mesoporous silicas functionalized with a high density of carboxylate groups as efficient adsorbents for the removal of basic dyes, *J. Mater. Chem.* 16 (2006) 2347–2353.
- [27] S.S. Gupta, K.G. Bhattacharyya, Kinetics of adsorption of metal ions on inorganic materials: A review, *Adv. Colloid Interface* 162 (2011) 39–58.
- [28] K.Y. Foo, B.H. Hameed, Insights into the modeling of adsorption isotherm systems, *Chem. Eng. J.* 156 (2010) 2–10.
- [29] M. Anbia, S.A. Hariri, Removal of methylene blue from aqueous solution using nanoporous SBA-3, *Desalination* 261 (2010) 61–66.
- [30] M.M. Mohamed, Acid dye removal: Comparison of surfactant-modified mesoporous FSM-16 with activated carbon derived from rice husk, *J. Colloid Interface Sci.* 272 (2004) 28–34.
- [31] T.M. Suzuki, M. Mizutani, T. Nakamura, Y. Akimoto, K. Yano, Pore-expansion of organically functionalized monodispersed mesoporous silica spheres and pore-size effects on adsorption and catalytic properties, *Microporous Mesoporous Mater.* 116 (2008) 284–291.
- [32] G. Halsey, Physical adsorption on non-uniform surfaces, *J. Chem. Phys.* 16 (1948) 931–937.
- [33] S.Y. Yoon, C.G. Lee, J.A. Park, J.H. Kim, S.B. Kim, S.H. Lee, J.W. Choi, Kinetic, equilibrium and thermodynamic studies for phosphate adsorption to magnetic iron oxide nanoparticles, *Chem. Eng. J.* 236 (2014) 341–347.
- [34] A. Özer, G. Akkaya, M. Turabik, The biosorption of Acid Red 337 and Acid Blue 324 on *Enteromorpha prolifera*: The application of nonlinear regression analysis to dye biosorption, *Chem. Eng. J.* 112 (2005) 181–190.
- [35] D. Karadag, E. Akgul, S. Tok, F. Erturk, M.A. Kaya, M. Turan, Basic and reactive dye removal using natural and modified zeolites, *J. Chem. Eng. Data* 52 (2007) 2436–2441.